IEEE Access
Multidisciplinary | Rapid Review | Open Access Journal

Received July 23, 2021, accepted August 8, 2021, date of publication August 11, 2021, date of current version August 18, 2021.

Digital Object Identifier 10.1109/ACCESS.2021.3104007

Fault Detection and Classification Scheme for PV System Using Array Power and Cross-Strings Differential Currents

F. M. ABOSHADY[1], (Member, IEEE), AND IBRAHIM B. M. TAHA[2]
[1]Electrical Power and Machines Engineering Department, Faculty of Engineering, Tanta University, Tanta 31512, Egypt
[2]Department of Electrical Engineering, College of Engineering, Taif University, Taif 21944, Saudi Arabia

Corresponding author: F. M. Aboshady (eng.aboshady@f-eng.tanta.edu.eg)

This work was supported in part by Taif University Researchers, Taif University, Taif, Saudi Arabia, under Project TURSP-2020/61.

ABSTRACT Accurate and fast fault monitoring system is important for photovoltaic (PV) systems to reduce the damage and energy loss associated with faults. This paper presents a fast fault detection and classification scheme for PV systems. The rate of change of the measured power at the array level is firstly used to detect and differentiate between shading and PV system short-circuit faults. Then, the measured cross-strings differential currents classify the fault type in the case of short-circuit faults. The proposed method accounts for intra-string, string-to-negative terminal, cross-string (string to string), and pole-to-pole short-circuit faults, as well as open circuit faults. Two current transducers per two strings are only required to apply the method leading to a significant reduction in the number of transducers/sensors compared to the literature, making it a cost-effective solution. The fault is detected and classified in 1 ms. A 400 kW PV system consisting of 4 arrays simulated using MATLAB/Simulink package is used for the evaluation process. Short-circuit faults are imposed at different conditions of mismatch levels and fault resistance values. Also, operation at reduced irradiance level is considered, and shading faults are simulated in different levels. The simulation results prove the ability of the proposed scheme to detect and differentiate between shading and short-circuit faults. The proposed method can correctly classify different fault types in almost all cases. The low implementation cost due to the lower number of required sensors and the fast-operating time (1 ms) boost the feasibility of the proposed method.

INDEX TERMS Fault classification, PV system, shading, short-circuit.

I. INTRODUCTION

The electric load demand is increasing, intending to electrify the transportation sector, which increases the need for more energy generation. The unfavorable environmental impacts of conventional generation plants hinder building new conventional units [1]. In 2019, the electricity generation sector in the United States of America was the second-highest source of greenhouse gases with 25% [2], and it accounted for 21% of emissions in the United Kingdom for the same year [3]. Renewable energy sources are the target for different countries as a clean energy source to tackle this problem [4], [5]. Renewable energy sources include photovoltaic (PV), hydro, wind, fuel cell, geothermal and tidal power plants [4], [5]. The PV power plants are considered a clean and promising source of energy [6]. However, PV power plants have two main drawbacks. The first is the high initial cost and the need for a wide construction area, while the second is the low operating efficiency [7].

Fault detection and classification techniques help preventing catastrophic failures in PV systems [8]. Some researchers relied on artificial intelligence techniques to detect and classify faults in PV systems [9]–[14]. The model presented in [9] suggested using two diodes connected at the upper and lower terminals of each string to facilitate the fault detection and classification. This method depended on using two current transducers for each string to measure the upper and lower currents. The detection algorithm was built based on both neural patterns recognition (NPR) and ensemble bagged trees (EN) algorithms. The main drawbacks of this method are related to using large number of diodes and sensors for large PV systems and a large number of samples is required for the training of both NPR

The associate editor coordinating the review of this manuscript and approving it for publication was Baoping Cai.

and EN algorithms. Furthermore, shading faults were not considered in [9].

In [10], graph-bass semi-superposed learning (GBSSL) technique was used to build a model used to detect and classify the fault types. The presented model was built to protect the PV system during the inverter side AC system faults. A large number of training samples (7488) were used for training the GBSSL model, which increased the simulation time. Furthermore, string to string, pole-to-pole, and shading faults were not considered. A model based on radial basis artificial neural network (RB-ANN) and fuzzy logic (FL) interface system was proposed in [11]. The faulty array and partial shading were only considered with detection accuracy up to 92.1%. The classification between high and low string faults, the string to string, pole-to-pole, and open circuit faults were not covered. Reference [12] suggested a random forest model for detecting the PV system faults. The cell-to-cell, degradation, open circuit, and partial shading faults were considered high detection and classification accuracy. The string to string, pole-to-pole, and complete shading faults were not considered. Also, it did not distinguish between low and high string faults, and a large dataset was required for the training process. The grey wolf optimizer (GWO) approach was used to detect and classify the PV system fault types [13]. The suggested GWO detection accuracy was compared with both the genetic algorithm and Tabu search algorithm. The short and open circuit faults were considered in this work, but pole-to-pole and shading faults were not considered. The effect of irradiance variations was not taken into consideration. In [14], the fuzzy logic interface (FL) algorithm was implemented for detecting and classifying the PV system fault types. The presented algorithm was used to detect shading, PV array, and hot spot faults, but it had a complexity to be implemented.

Another category of techniques depends on analyzing the voltage and current waveforms of the PV system [15]–[26]. In [15], a fault detection and classification technique based on scanning the I-V curve of the array has been reported. Firstly, the abnormal condition was detected based on comparing the disturbance in the current with a threshold level. Then, the fault was classified by initiating an order to trigger scanning the I-V curve to define the number of maximum power points and the presence of inflection points. The technique accounted for intra-string, cross-string, open circuit, and partial shading faults and did not consider string to the negative terminal and pole-to-pole faults. It was not clear if scanning the I-V curve was online or offline. The rate of change of voltage-current has been used in [16] to detect and classify different faults. This method depended on measuring the voltage and current of each string. The intra-string, cross-string, string to the negative terminal, pole-to-pole, and shading faults have been detected and classified but not open circuit fault. With two transducers per string, the implementation cost increases with large PV systems.

Reference [17] presented a fault detection model to detect cell to cell and cell to ground faults during normal and low irradiance and partial shading periods based on the maximum power point tracking (MPPT). The proposed model separates between normal and faulty states without separation between fault types. Open circuit, string to string, and pole-to-pole faults were not considered. In [18], a fault detection method was presented based on measuring the voltage of both the upper cell and the lower cell in each string and the total array voltage and current. The suggested model was used to identify and detect the string to string, the string to ground, open circuit faults, and partial shading faults. The main drawbacks of this model are evaluating many conditions for classifying each fault type, the complexity of the suggested algorithm, the irradiance effect has not been considered, and it did not separate between low and high fault levels. The model presented in [19] was built to detect and identify the PV system fault types based on the normalized super-imposed power component of the PV array. This method distinguished between short-circuit faults and partial shading without classifying the short-circuit fault types. In [20], a technique based on the difference between the maximum power tracking point for the simulated and the real PV arrays (output voltage, current, and power) has been proposed. It classified string and shading faults without distinguishing between low and high fault states. Also, this model did not consider the pole-to-pole faults and irradiance reduction effect on the PV system faults. In [21], the PV system fault detection model was built based on the local outlier factor of the string's current. The model was used for classifying sting, open circuit, and shading faults with different irradiance levels. The suggested model did not consider the pole-to-pole and string to string fault types and did not distinguish between low and high string faults. The fault detection model presented in [22] relied on an optimal number of voltage sensors required for a PV system connected to an AC grid. The model is only used to detect the short circuit faults of each string. The complexity of the suggested model to determine the fault location in each string with the lack of detection of string to string, pole-to-pole, and open circuit faults represent the main drawbacks of this model. In [23], a fault detection method based on the PV system power losses and current and voltage indicators was reported. The model focused only on detecting the PV system faults during the partial shading and the inverter maloperation periods. This model is valid during low irradiance periods and cannot be implemented to detect faults during normal irradiance conditions. A simple PV system fault detection technique was presented in [24] based on the array voltage and current besides the irradiance and temperature sensors. Threshold values for voltage and current were determined considering the PV system configurations. The threshold values were used for detecting string fault types. The open circuit, pole-to-pole and shading faults as well as the irradiance effect were not considered in this work. The model presented in [25] is based on the power loss in the PV system. The suggested model diagnosed the PV system grounding, string short circuit, blocking diode failures and shading faults. The detection algorithm ignored the string

open circuit, the complete string shadow, and the irradiance reduction. In [26], a detection method that used temperature and irradiance sensors and power meter for each string to diagnose the short and open circuit faults has been presented. The suggested algorithm detected only string cell to cell and open circuit faults and ignored the other fault types.

The literature shows the shortage in the existing fault detection and classification techniques for PV systems. For instance, some techniques ignored many fault types while some other techniques use two sensors for each string which increases the implementation cost. Also, some techniques are complex. This paper proposes a simple and fast fault detection and classification model to overcome the limitations in the literature. The proposed method uses the rate of change of the measured power at the array level to detect and distinguish between shading and PV system short-circuit faults. Cross-strings differential currents are used to classify the short-circuit faults. The proposed method is efficient for detecting intra-string, string-to-negative terminal, cross-string (string to string), pole-to-pole short-circuit faults, and open circuit faults. Two current transducers per two strings are only required to apply the method, leading to a significant reduction in the number of transducers/sensors compared to the literature, making it a cost-effective solution. A 400 kW PV system consisting of four arrays simulated using MATLAB/Simulink package is used for the evaluation process. Short-circuit faults are imposed at different conditions of mismatch levels and fault resistance values. Furthermore, operations at different irradiance levels are considered for short-circuit and shading faults. The proposed technique has the following features:

- It can detect and classify different fault types (intra-string, cross-string (string to string), string-to-negative terminal, pole-to-pole, shading, and open circuit) at different irradiance and fault resistance levels.
- It uses only one current transducer per string. It significantly reduces the implementation cost compared to the existing methods.
- Fast operation as it operates in 1 ms.
- It can easily be applied to different PV system sizes as the controlling parameters are calculated from either the PV system parameters or through simple simulation studies.

II. PROPOSED METHOD

A. CONCEPT AND REQUIRED MEASUREMENTS

The proposed protection and monitoring system depends on measuring the differential current between every two strings' upper and lower terminals. To illustrate this concept, consider two strings with upper and lower currents, as shown in Fig. 1. The proposed method measures the differential current (I_{d1}) between the upper current (I_{11}) and the lower current (I_{22}) of two neighboring strings and the differential current (I_{d2}) between the two other currents (I_{12} and I_{21}).

The differential current can be measured using a single current transducer (CT), where the two current-carrying conductors pass through the transducer hole. Therefore, for every two strings, two CTs are used.

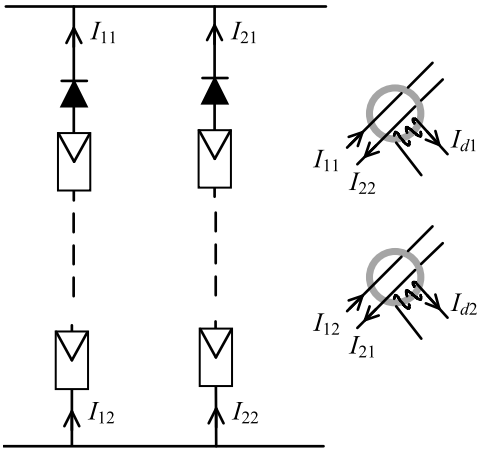

FIGURE 1. Proposed protection system using the differential current approach.

B. PERFORMANCE DURING INTRA-STRING FAULT

When a fault occurs between terminals of a single or a group of modules in the same string, the blocking diode prevents the reverse current flow and isolates this string from the system. The current in the faulty module(s) increases while the upper and lower currents in the faulty string become zero, as shown in Fig. 2. The other healthy strings continue to operate normally, and their currents are not affected by this type of fault. The upper and lower currents of the two neighboring strings and the expected differential currents can be summarized as follows:

$$\begin{aligned} I_{11} &= I_{12} = 0 \\ I_{21} &= I_{22} = I_m \\ |I_{d1}| &= |I_{11} - I_{22}| \\ |I_{d2}| &= |I_{12} - I_{21}| \\ |I_{d1}| &= |I_{d2}| = I_m \end{aligned} \tag{1}$$

where I_m is the current in the healthy string, the string current is at the maximum power point (MPP).

Depending on the fault resistance value and the number of faulty modules, the current generated by the fault module(s) is divided between the fault branch (I_F) and the string current (I_{11}). Therefore, the upper and lower currents in the faulty string decrease significantly but not to zero. In this case, the differential currents (I_{d1}) and (I_{d2}) will be less than the healthy string current (I_m). However, the two differential currents are still large and equal. The fault is classified as intra-string LOW for this case. On the other hand, the first case where the whole current passes through the fault branch is classified as intra-string HIGH. For the HIGH fault case, the number of modules participating in the fault is large, for the same fault resistance, compared to the intra-string LOW case, which means more damage if the fault is not accurately detected.

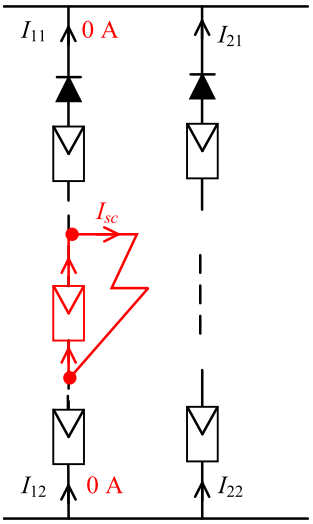

FIGURE 2. System configuration with an intra-string fault.

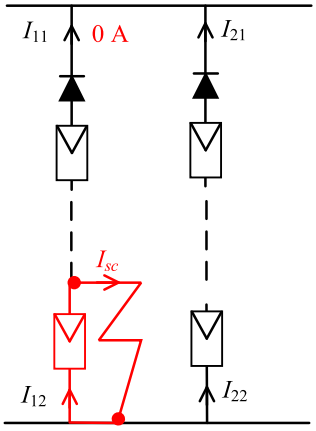

FIGURE 3. System configuration with a string-to-negative terminal fault.

C. PERFORMANCE DURING STRING-TO-NEGATIVE TERMINAL FAULT

In this case, the fault occurs between a module in the string and the negative terminal current-carrying conductor, as depicted in Fig. 3. Like the intra-string case, the diode isolates the string preventing any reverse current infeed. However, the lower side current in the fault string holds the whole fault current and the module short-circuit current (I_{sc}). The four currents of interest and the corresponding two differential currents are given by (2). The first differential current has a high value, but the second differential current is small. As is clear, the relation between the values of the differential currents for this fault case is different from the intra-string case. Therefore, the two differential currents can be used to distinguish between the two fault types.

$$\begin{aligned} I_{11} &= 0 \\ I_{12} &= I_{sc} \\ I_{21} &= I_{22} = I_m \\ |I_{d1}| &= I_m \\ |I_{d2}| &= |I_{sc} - I_m| \end{aligned} \tag{2}$$

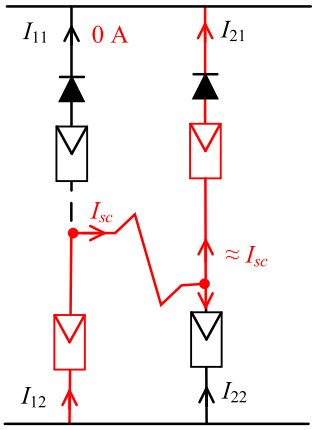

FIGURE 4. System configuration with a cross-string fault.

The string-to-negative terminal fault is also split into HIGH and LOW. For higher fault resistance values or the small number of modules included in the fault, the upper current in the faulty string (I_{11}) will not be zero. This, in turn, decreases the value of (I_{d1}) to be less than the healthy string current (I_m), and the fault is classified as string-to-negative LOW.

D. PERFORMANCE DURING CROSS-STRING FAULT

Cross-string fault occurs between two strings, as shown in Fig. 4. The direction of the fault current depends on the relative number of modules participating in the fault from the two strings. Assuming the number of lower modules in the left-hand side string is higher than those in the right-hand side string, the fault current path will be shown in Fig. 4.

The upper current in the left-hand side string (I_{11}) decreases to zero due to the diode effect, while the lower current (I_{12}) increases to the short-circuit current (I_{sc}). Most of the fault current passes through the upper part of the right-hand side string (I_{21}) with a very low current return to the left-hand side string through the lower part of the right-hand side string (I_{22}). Accordingly, the differential currents can be estimated by (3). Unlike the intra-string and string-to-negative terminal faults, both differential currents have small values for the cross-string faults. Therefore, the cross-string fault can be differentiated from the other two fault types. The fault is classified as cross-string HIGH for this case.

For a cross-string LOW fault, the current (I_{11}) does not decrease to zero but will be a portion of the lower current (I_{12}). Also, the current (I_{22}) is not reversed. The two differential currents (I_{d1}) and (I_{d2}) slightly increase but are still not as high as their values with the intra-string LOW faults.

$$\begin{aligned} I_{11} &= 0 \\ I_{12} &= I_{sc} \\ I_{21} &\cong I_{sc}(\text{a little bit} < I_{sc}) \\ I_{22} &= \text{small value} \\ |I_{d1}| &= |I_{11} - I_{22}| = \text{small value} \\ |I_{d2}| &= |I_{12} - I_{21}| = \text{small value} \end{aligned} \tag{3}$$

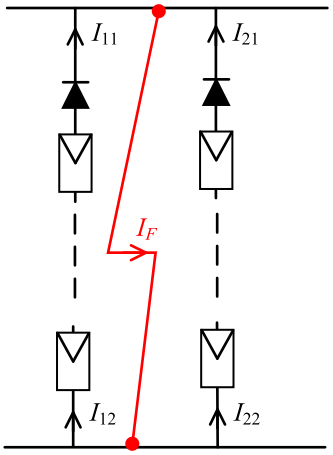

FIGURE 5. System configuration with a pole-to-pole fault.

E. POLE-TO-POLE FAULT

For a fault between the positive and negative terminals (pole-to-pole) as depicted in Fig. 5, high current flows through the fault path coming from different strings leading to significant loss in the whole array output power. The measured differential currents will be zero during this fault assuming equal pre-fault currents in the strings.

F. OPEN CIRCUIT FAULT

An open circuit in a string leads to zero current getting out from this string which is similar to an intra-string HIGH fault (refer to Fig. 2 and (1)). Accordingly, the performance of the proposed method is similar for both open circuit and intra-string HIGH faults, and the faulted string can be located. The open-circuit fault causes a reduction in the array output power without damage in the string's modules because the current is zero.

G. SHADING FAULT

It is important to distinguish between short-circuit faults and temporary shading because the latter does not require system interruption. The distinct feature for the shading fault is the low rate of change of power (RoCoP). During short-circuit faults, the RoCoP is very high, and the power changes almost instantaneously. On the other hand, the shading requires a longer time (low RoCoP) that can be as high as few hundreds of milliseconds or even in seconds [15]. Fig. 6 shows the change in the output power from a PV system during a short-circuit fault and a shading fault on a string (irradiance changes from 1000 to 200 W/m^2 within 100 ms). Even if the shading has been simulated to be as fast as 100 ms, it is very slow compared to the short-circuit fault. The RoCoP at the array level (or the inverter level) where the power is inherently measured is used as a detector to distinguish between shading and short-circuit faults. Then, the proposed current differential scheme is implemented to classify the fault type.

The RoCoP is calculated using two measurement samples by (4), where k is the sample number and T_s is the measurement sampling time. The threshold value for the RoCoP, used to distinguish between shading and short-circuit, can be estimated from the worst-case scenario for a shading fault. Assume the power has changed during the shading fault as depicted in Fig. 6. The maximum RoCoP for this shading fault corresponds to the maximum possible change in the power and the minimum possible shading time. Numerical threshold is given later in the performance evaluation section.

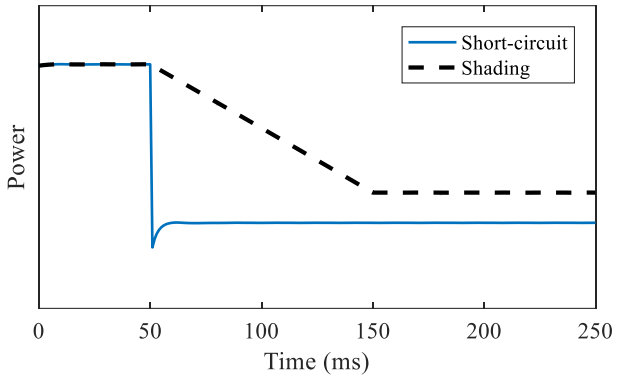

FIGURE 6. Output power during short-circuit and shading.

$$|RoCoP| = \frac{|P(k) - P(k-1)|}{T_s} \tag{4}$$

H. FAULTS DURING REDUCED IRRADIANCE LEVEL

The previous analysis for the short-circuit faults considers zero differential currents before the fault inception. Suppose one of the two strings operates at a reduced irradiance level due to shading. In that case, there will be a difference in the strings currents, and the measured differential currents will not be zero during the non-fault (healthy) condition. Of course, the shading will be detected while it is occurring, based on the RoCoP. However, the case intended here concerns short-circuit occurrence after the shading becomes stable. Here are two points to consider.

The first point is the discrimination between the cross-string fault and the other fault types. As previously mentioned, the differential currents are small during the cross-string fault (refer to (3)). With the mentioned effect of reduced irradiance, the differential currents may not be small during the healthy condition and will not be small when a cross-string fault occurs. However, the increment in the differential current due to the cross-string fault is what will be small. Therefore, to distinguish between cross-string fault and other types, the incremental differential current (ΔI_d) is used, which is the difference between two successive samples.

The second point is the classification of the fault as HIGH or LOW for both the intra-string fault and the string-to-negative terminal fault. The classification depends on the relative value of the differential currents with respect to the rated current at MPP (I_m) as previously explained and given in (1) and (2). For HIGH faults, both differential currents are equal to I_m for an intra-string fault, and one of the two

differential currents is equal to I_m for a string-to-negative terminal fault. However, suppose the fault occurs on a string while the neighbor healthy string operates at a low irradiance level. In that case, the differential currents will be less than I_m even if the fault is HIGH because the current in the healthy string is less than the rated I_m. The fault will incorrectly be classified as LOW when using I_m as the threshold value to differentiate between HIGH and LOW faults.

An adaptive threshold level is proposed to classify HIGH and LOW faults for the intra-string and string-to-negative terminal faults to overcome this problem. As previously mentioned, the pre-fault differential current is not zero for this situation. This pre-fault differential current $\boldsymbol{I_d^{pre}}$ is used to calculate the threshold current I_{th0} as (5), which is used to distinguish HIGH from LOW faults. It is proposed to consider a margin of 5% to account for possible fault transient effects. If the differential current during the fault period is greater than the threshold current I_{th0}, then the fault is HIGH. Otherwise, the fault is classified as LOW.

$$I_{th0} = 0.95 \times (I_m - I_d^{pre}) \tag{5}$$

It is worth noting that in case the two strings operate at the same low irradiance level, the pre-fault differential current will be zero, and the proposed method may not be able to differentiate between HIGH and LOW faults. However, the fault is still classified as one of the main fault types but not as HIGH or LOW. The PV systems usually have irradiance sensors installed at different locations for the purpose of maximum power extraction. The irradiance value measured by these sensors can be used to update the current value at the MPP in the proposed method to further enhance the system performance.

In order to distinguish normal system operation from the previously explained fault types, the RoCoP at the array is used. In normal conditions, the power slightly oscillates around the maximum power-point. The change in the power is very little and is a function of the MPPT algorithm used. Therefore, a small RoCoP value (RCP_H) is used to differentiate between normal and abnormal conditions. The flowchart in Fig. 7 illustrates the procedure for fault detection and classification. This procedure is implemented on every two strings in the system. Therefore, the fault location is also identified.

The threshold values (RCP_H, RCP_{th}, I_{th1}, and I_{th2}) used to classify the fault type in the flowchart are determined from simulating faults at different conditions, as illustrated later in the simulation studies.

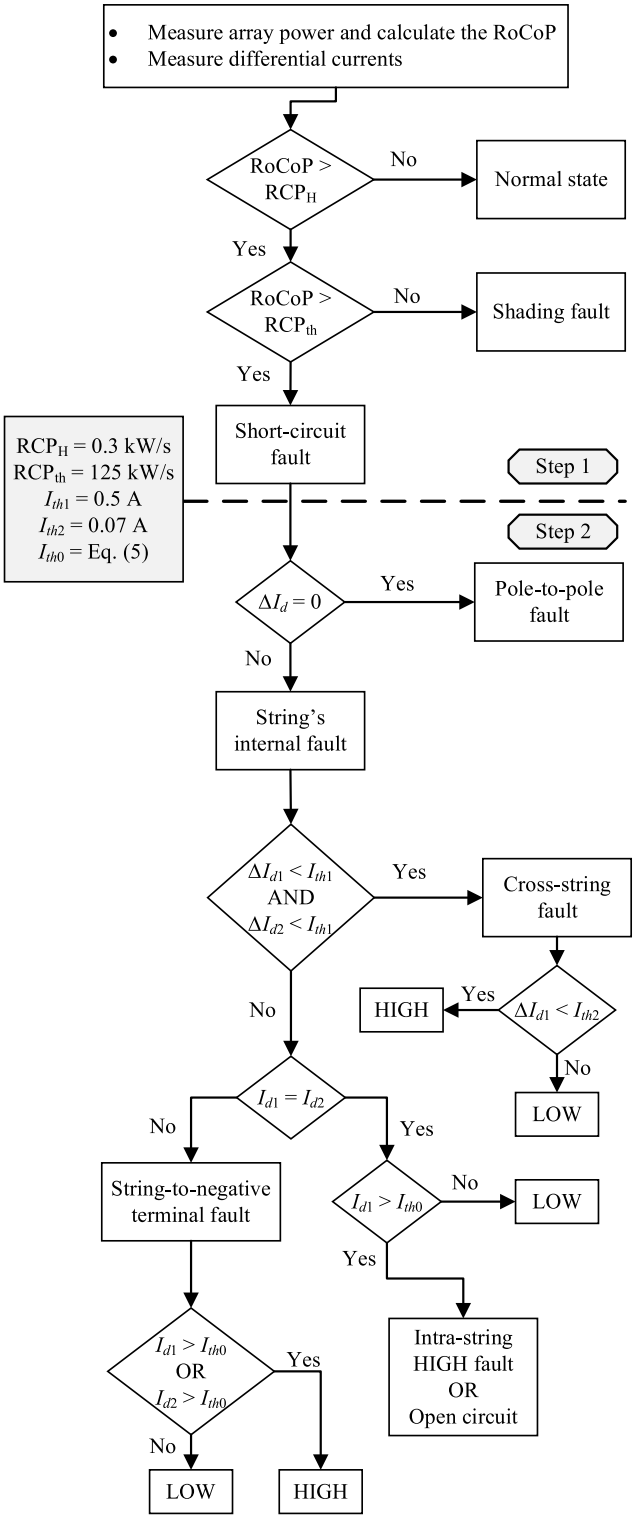

FIGURE 7. The procedure of the proposed scheme.

III. PERFORMANCE EVALUATION

A. SYSTEM DESCRIPTION

The 400-kW grid-connected PV farm available in the MATLAB/Simulink which is shown in Fig. 8, is used in this study [27]. The PV farm has four arrays of 100 kW each. Each array has 64 parallel strings with five series-connected modules per string. Table 1 shows the parameters of a single PV module and the parameters of the system. The farm is connected to a 25 kV distribution grid and a 120 kV transmission grid through step-up transformers, which are not shown in Fig. 8 and are considered as part of the main grid block. The maximum power is extracted from each array using the Perturb and Observe maximum power point

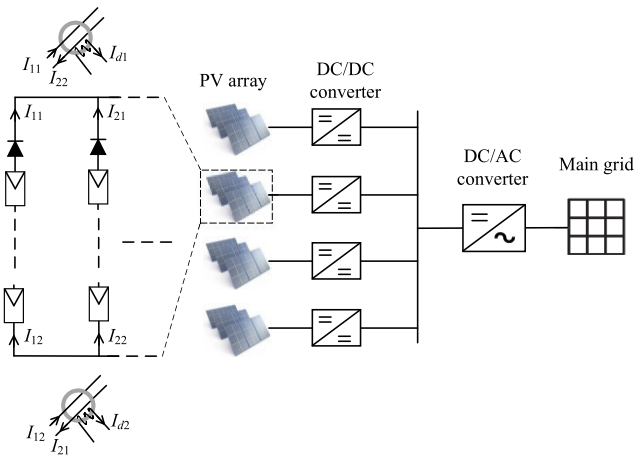

FIGURE 8. Construction of the simulated 400 kW PV system.

TABLE 1. Parameters of the system.

Parameter	Value
PV module maximum power	315 W
PV module MPP current	5.76 A
PV module MPP voltage	54.7 V
PV module Short-circuit current	6.14 A
PV module Open-circuit voltage	64.6 V
PV module Shunt resistance	430 Ω
PV module Series resistance	0.43 Ω
DC/AC converter	500 V DC to 260 V AC
AC system frequency	60 Hz
AC low voltage series RL filter	1 m Ω, 45μH
AC low voltage shunt C filter	260 V, 40 kVAR
Coupling transformer	400 kVA 260 V/25 kV
Distribution grid voltage	25 kV
Transmission grid voltage	120 kV

tracking (MPPT) technique implemented with each DC/DC converter.

Assuming in worst case, the shading results in a reduction in the total array power by 50 kW (half the total array power) in 0.5 s. The corresponding RoCoP is 100 kW/s. Considering a safety margin of 25% between the shading and the short-circuit faults, a threshold value (RCP_{th}) of 125 kW/s is used in this paper to distinguish shading from short-circuit faults. The simulation study shows that the RoCoP under normal conditions does not exceed 0.3 kW/s. Therefore, this value is used as the setting for RCP_H.

B. ILLUSTRATIVE CASES

This section illustrates the operation of the proposed scheme by simulating different shading and short-circuit faults.

1) SHADING FAULTS

Shading occurs due to different reasons, including passing clouds and nearby buildings. Shading has been simulated as a decrease in the irradiance level with a specified rate of change. In [15], it has been assumed that the irradiance changes from 1000 W/m^2 to 800 W/m^2 in 2 s to simulate

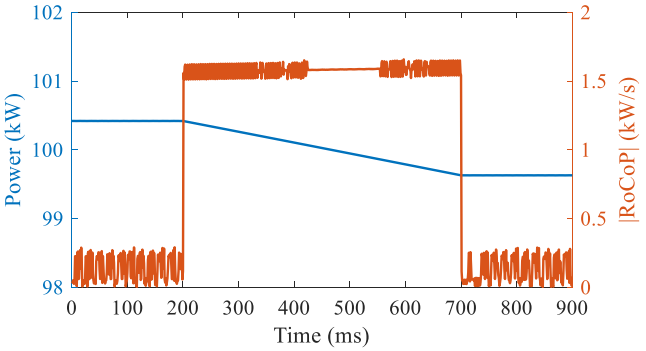

FIGURE 9. Measured array power and calculated RoCoP for uniform shading fault affecting one string.

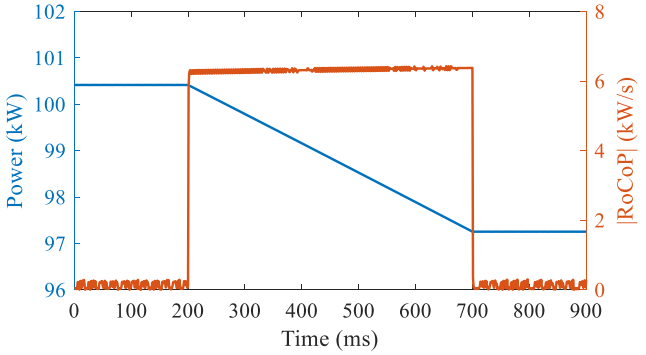

FIGURE 10. Measured array power and calculated RoCoP for uniform shading fault affecting four strings.

the shading effect. This paper has assumed that the irradiance level decreases in 0.5 s, which is four times faster than [15].

Three uniform shading cases have been simulated where the irradiance changed from 1000 W/m^2 to 500 W/m^2, and the shading affected one string, four strings, and the whole array's strings in addition to simulating two partial shading cases at higher irradiance levels (1000 W/m^2 to 700 W/m^2), which affected only two modules of the string. The partial shading has been imposed on three strings and six strings. The measured array power and the calculated RoCoP for different cases are shown in Fig. 9, Fig. 10, Fig. 11, Fig. 12, and Fig. 13. The RoCoP value increases with increasing the affected strings. Nevertheless, the RoCoP for all cases did not exceed the threshold RoCoP ($RCP_{th} = 125$ kW/s). Accordingly, these test cases were identified as shading, not short-circuit faults, and the proposed method can identify both uniform and partial shading.

2) SHORT-CIRCUIT STRING FAULTS

Different string short circuit fault categories considered in this paper have been simulated with a fault resistance of 1 Ω and 20 Ω to illustrate the performance of the proposed method for both HIGH and LOW faults. These faults are shown in Fig. 14. The first fault is an intra-string with two modules involved in the fault, the second is a string-to-negative terminal between the second module and the negative terminal, and the third is a cross-string fault from module 4 in one string to module 2 in the other string.

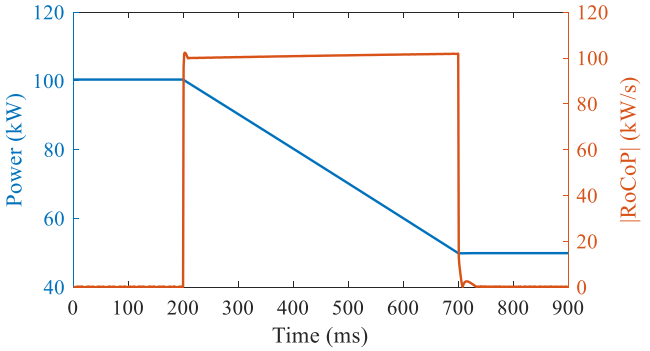

FIGURE 11. Measured array power and calculated RoCoP for uniform shading fault affecting a whole array (64 strings).

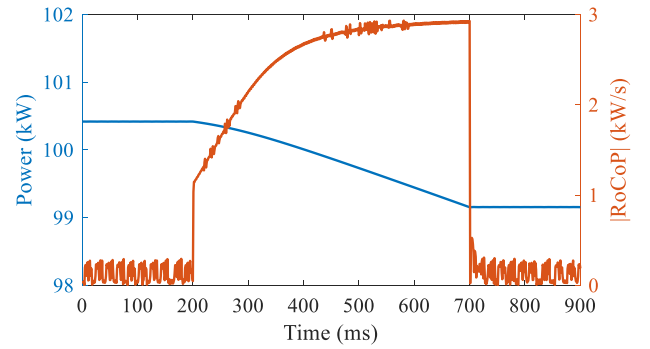

FIGURE 12. Measured array power and calculated RoCoP for partial shading fault affecting three strings.

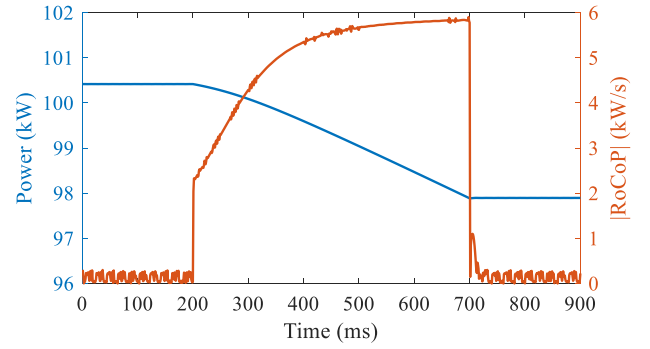

FIGURE 13. Measured array power and calculated RoCoP for partial shading fault affecting six strings.

Each of the three faults has a mismatch level of 2 modules. The differential currents are measured with a sampling frequency of 1 kHz.

For the intra-string fault with a resistance of 1 Ω, Fig. 15 shows the array power and the corresponding RoCoP. The RoCoP value (1815 kW/s) is high once the fault occurs and much higher than the threshold value (125 kW/s). Therefore, the fault is detected and classified as a short-circuit fault. The second step is to classify the fault based on the differential currents. The measured differential currents are shown in Fig. 16. The two differential currents are equal during the fault. During the fault steady state, the two differential currents are equal to the current at the MPP. The first sample of during fault current i.e., after 1 ms, is a little higher than the current at the MPP because of the fault transient. Because the two differential currents are close to the current at the MPP I_m (higher than the threshold current $I_{th0} = 0.95I_m = 5.47$ A), this fault is classified as an intra-string HIGH. This result matches the analysis provided in the methodology section.

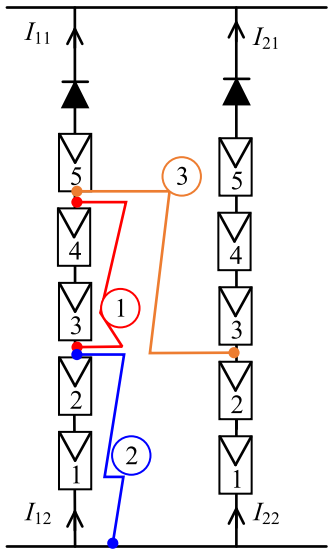

FIGURE 14. An illustrative example for different short-circuit fault types.

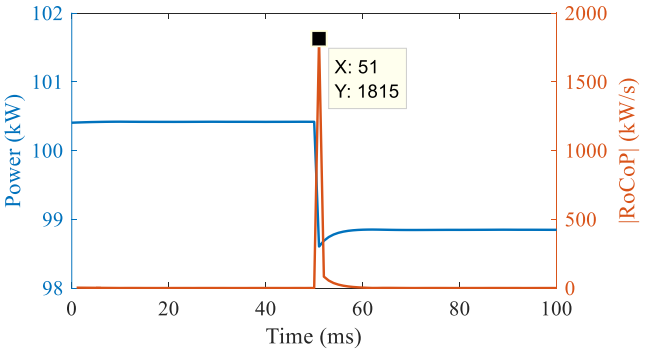

FIGURE 15. Measured array power and calculated RoCoP for an intra-string fault with a resistance of 1 Ω.

Fig. 17 and Fig. 18 show the array power and RoCoP and the measured differential currents for the intra-string fault with a resistance of 20 Ω. The calculated RoCoP is 1144 kW/s which is higher than the threshold value (125 kW/s). The pre-fault differential currents are zero, and both during fault differential currents are equal to 3.87 A, which is less than the threshold current I_{th0} (5.47 A). Therefore, this fault is classified as an intra-string LOW which is the correct classification.

Regarding the string-to-negative terminal faults, Fig. 19 and Fig. 20 show the result for a fault resistance of 1 Ω while the result for the 20 Ω fault resistance is given in Fig. 21 and Fig. 22. For both cases, the calculated RoCoP is much higher than the threshold value (125 kW/s) which means they are classified as short-circuit faults. For the two cases, the two differential currents are neither low nor equal.

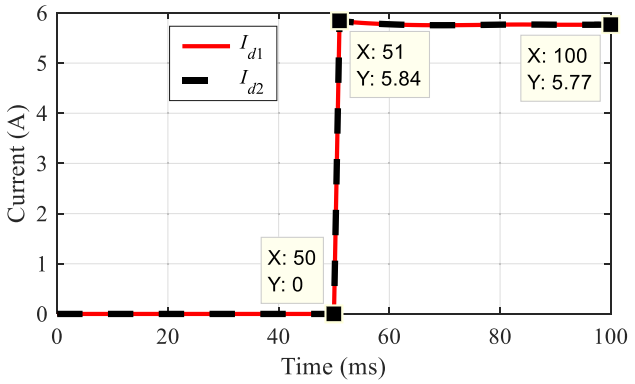

FIGURE 16. Measured differential currents for an intra-string fault with a resistance of 1 Ω.

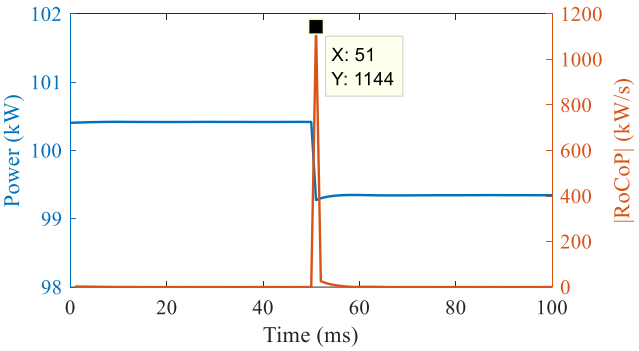

FIGURE 17. Measured array power and calculated RoCoP for an intra-string fault with a resistance of 20 Ω.

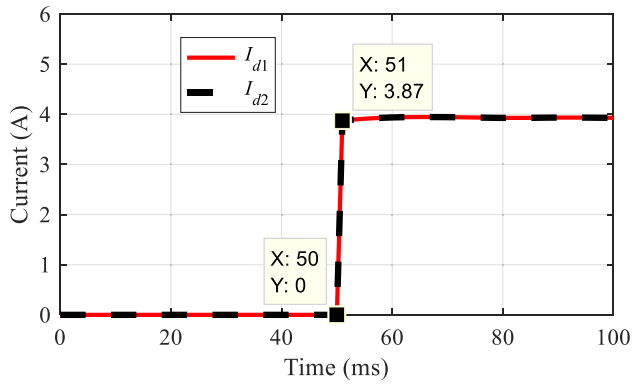

FIGURE 18. Measured differential currents for an intra-string fault with a resistance of 20 Ω.

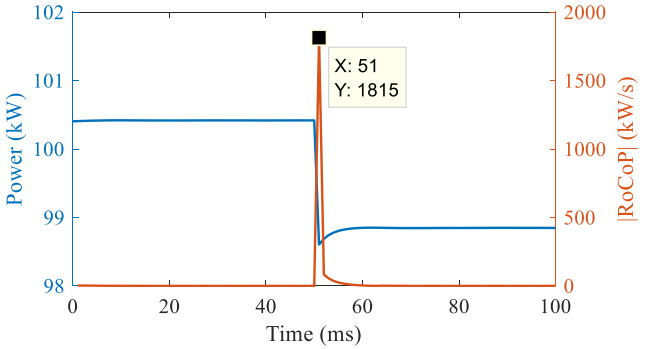

FIGURE 19. Measured array power and calculated RoCoP for a string-to-negative terminal fault with a resistance of 1 Ω.

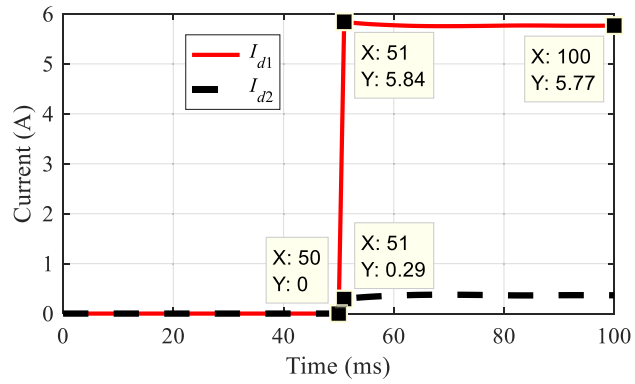

FIGURE 20. Measured differential currents for a string-to-negative terminal fault with a resistance of 1 Ω.

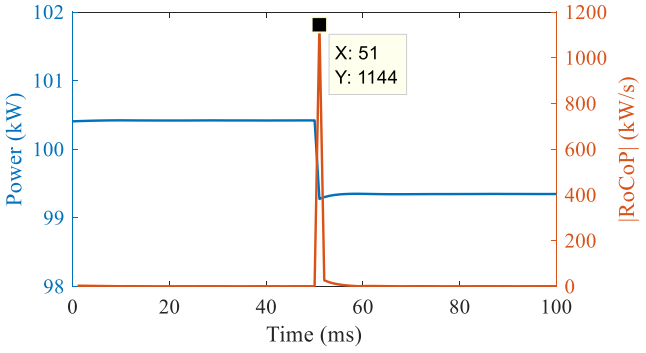

FIGURE 21. Measured array power and calculated RoCoP for a string-to-negative terminal fault with a resistance of 20 Ω.

Therefore, the two cases correspond to string-to-negative terminal faults following the procedure in Fig. 7. Because one of the differential currents during the fault (I_{d1} in this case) is close to the current at the MPP for the 1 Ω fault case (higher than the threshold current $I_{th0} = 0.95I_m = 5.47$ A), it is classified as HIGH fault. On the other hand, for the second case I_{d1} is lower than the threshold current I_{th0} (5.47 A) which means it is a LOW fault case. The first sample of during fault data has been used for the classification process which means the method is as fast as 1 ms (one sampling period).

The results for the cross-string two fault cases are depicted in Fig. 23, Fig. 24, Fig. 25, and Fig. 26. Similar to the previous short-circuit faults, the RoCoP values for these two cases are higher than the threshold RoCoP. The two differential currents during the fault are small (smaller than $I_{th1} = 0.5$ A), meaning that these fault cases correspond to cross-string faults following the procedure in Fig. 7. The current threshold value (0.5 A) has been defined from testing the system at various fault conditions. To differentiate between the HIGH and LOW faults, a threshold value of 0.07 A has been used, also identified from testing the system. Therefore, the fault case with 1 Ω resistance is classified as HIGH, while the other case is LOW.

The previous six test cases ensure the ability of the proposed method using the differential currents to distinguish between different string short-circuits fault types.

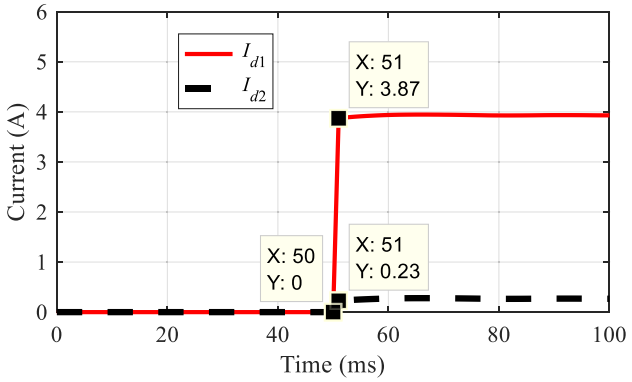

FIGURE 22. Measured differential currents for a string-to-negative terminal fault with a resistance of 20 Ω.

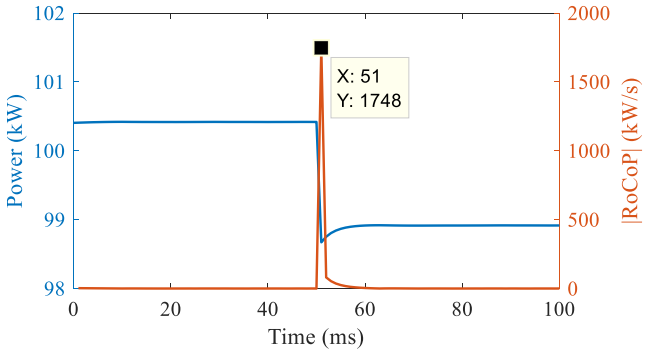

FIGURE 23. Measured array power and calculated RoCoP for a cross-string fault with a resistance of 1 Ω.

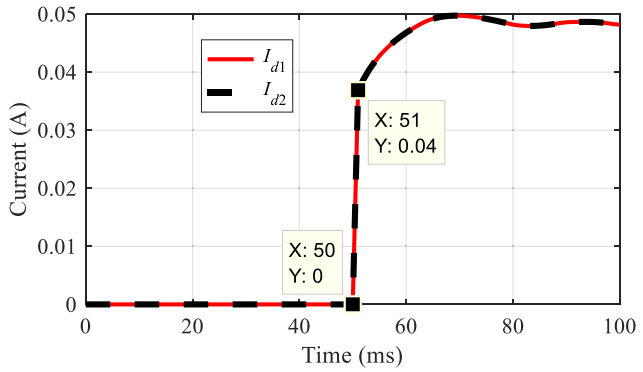

FIGURE 24. Measured differential currents for a cross-string fault with a resistance of 1 Ω.

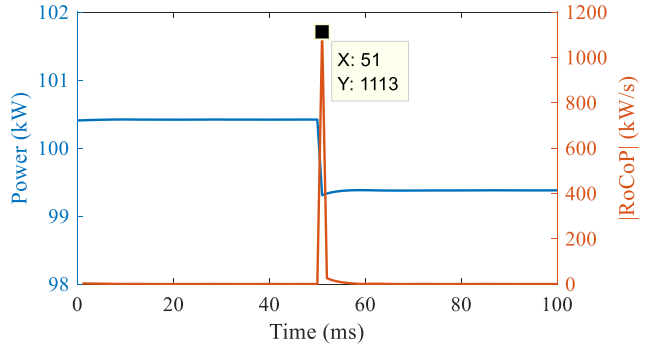

FIGURE 25. Measured array power and calculated RoCoP for a cross-string fault with a resistance of 20 Ω.

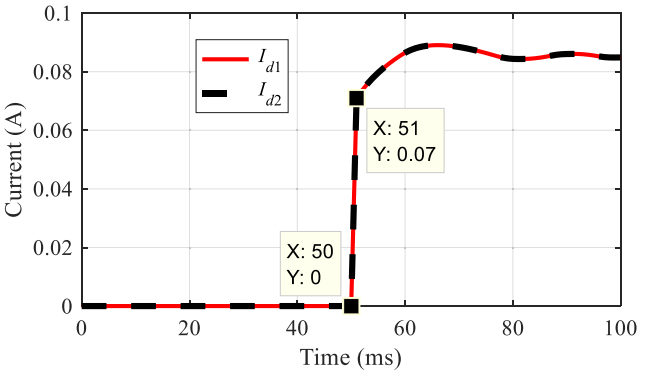

FIGURE 26. Measured differential currents for a cross-string fault with a resistance of 20 Ω.

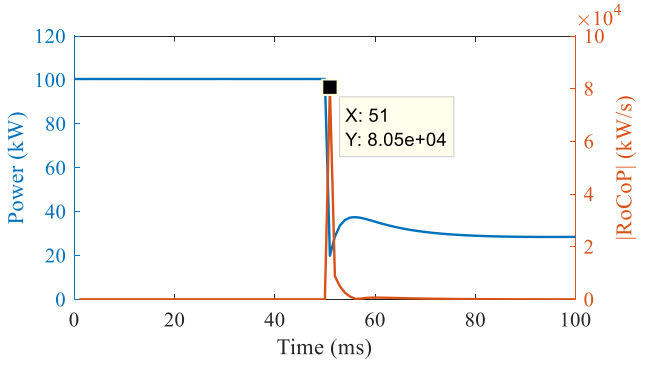

FIGURE 27. Measured array power and calculated RoCoP for a pole-to-pole fault with a resistance of 1 Ω.

3) POLE-TO-POLE FAULT

A fault has been imposed between the positive and negative terminals with a resistance of 1 Ω. The array output power significantly decreased, as shown in Fig. 27, and the corresponding RoCoP is extremely high (≈80500 kW/s). Because the fault is not internal for the strings, the differential current has not changed and is equal to zero. Therefore, this very high RoCoP, together with all strings that have no change in the current, is used to detect and classify the fault as pole-to-pole fault following the procedure in Fig. 7. The fault has been repeated with a resistance of 20 Ω, and the results are shown in Fig. 29 and Fig. 30, which also reflect the fault type as a pole-to-pole fault.

4) REDUCED IRRADIANCE

In the previous short-circuit fault cases, the two strings were subjected to the standard irradiance level (1000 W/m^2). To check the performance when one of the two strings operates at a lower irradiance level, the right-hand side string in Fig. 14 has been subjected to an irradiance of 700 W/m^2. The intra-string, string-to-negative terminal, and cross-string faults with a resistance of 1 Ω have been repeated at this new irradiance condition. The measured array power and the calculated RoCoP are shown in Fig. 31, Fig. 32, and Fig. 33 for the three fault cases. The RoCoP value is much higher than the threshold RoCoP (125 kW/s) for the three cases. Therefore, they are identified as short-circuit faults.

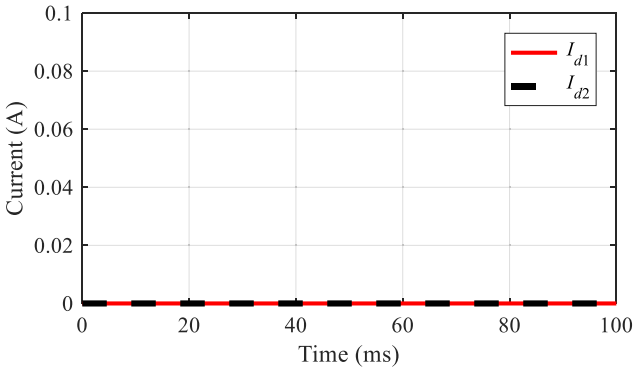

FIGURE 28. Measured differential currents for a pole-to-pole fault with a resistance of 1 Ω.

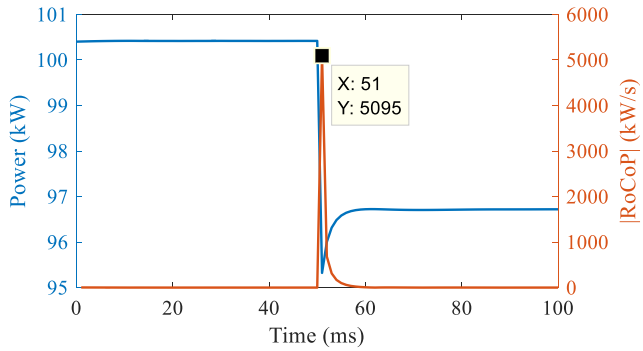

FIGURE 29. Measured array power and calculated RoCoP for a pole-to-pole fault with a resistance of 20 Ω.

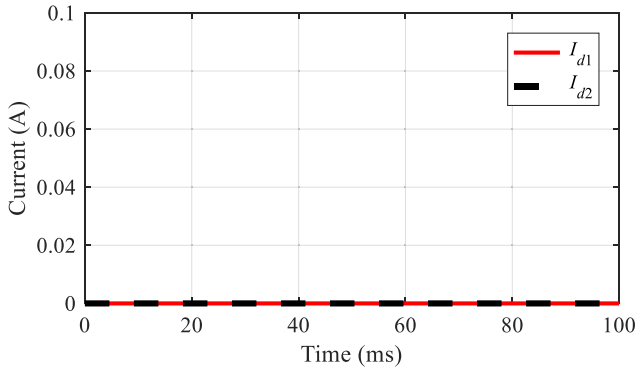

FIGURE 30. Measured differential currents for a pole-to-pole fault with a resistance of 20 Ω.

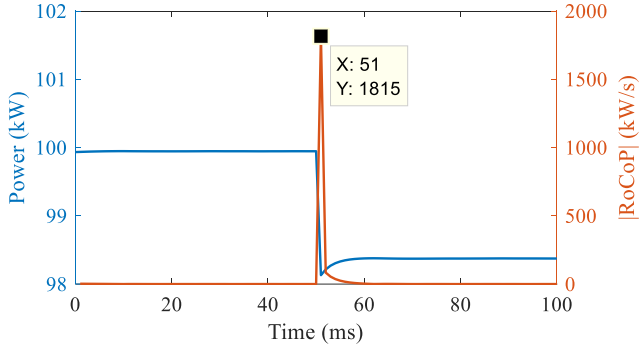

FIGURE 31. Measured array power and calculated RoCoP for an intra-string fault with a resistance of 1 Ω at reduced irradiance level.

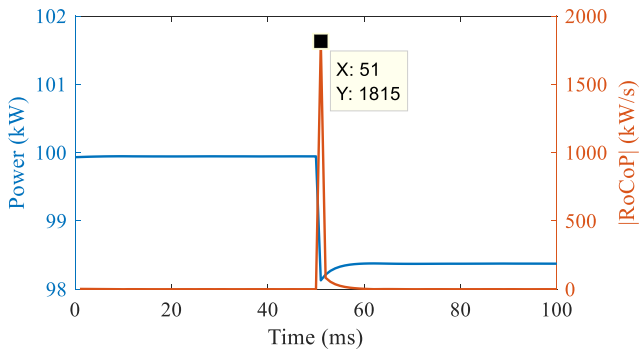

FIGURE 32. Measured array power and calculated RoCoP for a string-to-negative terminal fault with a resistance of 1 Ω at reduced irradiance level.

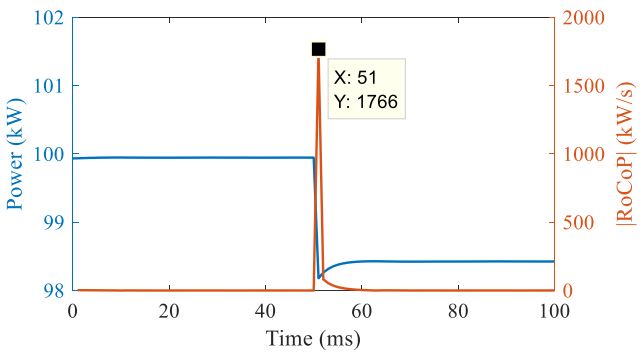

FIGURE 33. Measured array power and calculated RoCoP for a cross-string fault with a resistance of 1 Ω at reduced irradiance level.

The measured differential currents are shown in Fig. 34, Fig. 35, and Fig. 36. The pre-fault differential currents are not zero due to variance in irradiance between the strings, as previously explained. In terms of classifying the fault type, the incremental differential current when the fault occurred is ($\Delta I_d = 4.09 - 1.74 = 2.35$ A) for the intra-string and string-to-negative terminal faults. At the same time, it is 0.1 A for the cross-string fault. Comparing the incremental, differential current with the threshold level ($I_{th1} = 0.5$ A) as proposed in Fig. 7, the three fault cases are correctly attached to the right fault category. In terms of classifying the fault as HIGH or LOW, the threshold current I_{th0} is calculated by (5) as 3.82 A. Because the during fault differential current is greater than 3.82 A for both intra-string and string-to-negative terminal fault cases, then the two cases are classified as HIGH faults. On the other hand, the incremental current for the cross-string fault is equal to 0.1 A, which is higher than the threshold current ($I_{th2} = 0.07$ A). Therefore, the cross-string fault is classified as LOW, which is not the correct classification.

In addition to the previous test cases, the intra-string fault with a resistance of 1 Ω has been repeated at a lower irradiance level of 300 W/m^2. The array power and the RoCoP are shown in Fig. 37, indicating a short-circuit fault. The measured differential current in Fig. 38 is used to

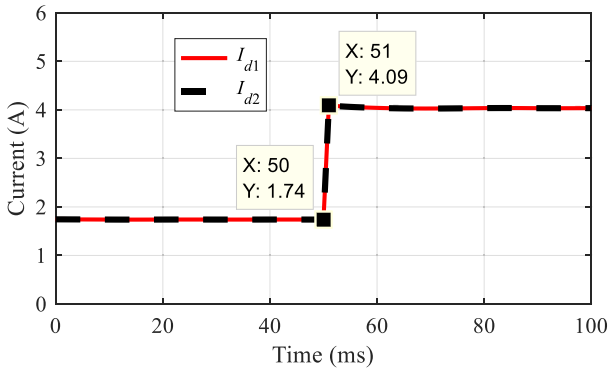

FIGURE 34. Measured differential currents for an intra-string fault with a resistance of 1 Ω at reduced irradiance level.

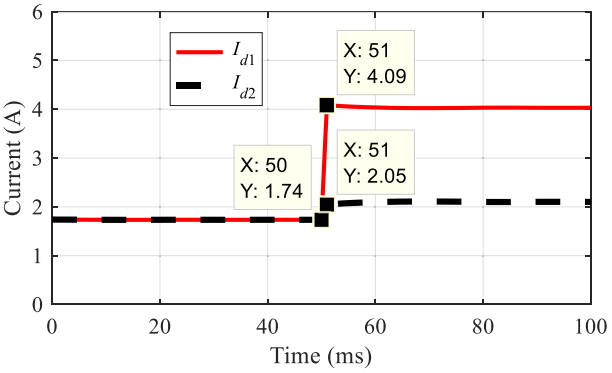

FIGURE 35. Measured differential currents for a string-to-negative terminal fault with a resistance of 1 Ω at reduced irradiance level.

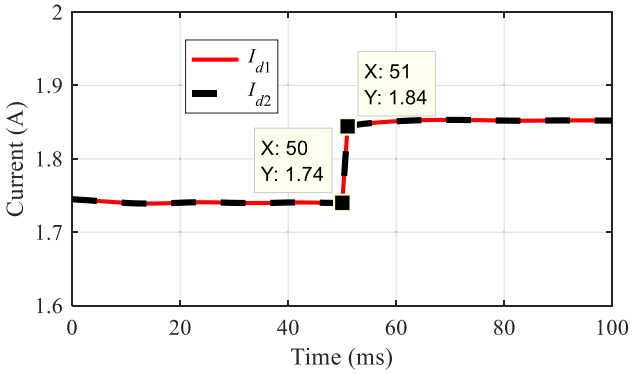

FIGURE 36. Measured differential currents for a cross-string fault with a resistance of 1 Ω at reduced irradiance level.

calculate the threshold current I_{th0} using (5) as 1.6 A. Because during the fault period, the differential current is 1.73 A (i.e., greater than I_{th0}), the fault is classified as an intra-string HIGH.

The results obtained from this test ensure the ability of the proposed method to classify the fault to the main categories (intra-string, string-to-negative terminal, and cross-string) based on the incremental differential current. Also, classifying the intra-string and string-to-negative terminal faults to HIGH and LOW using the adaptive threshold setting while it may fail, as happened for the studied case, to further classify the cross-string to HIGH or LOW under low irradiance level.

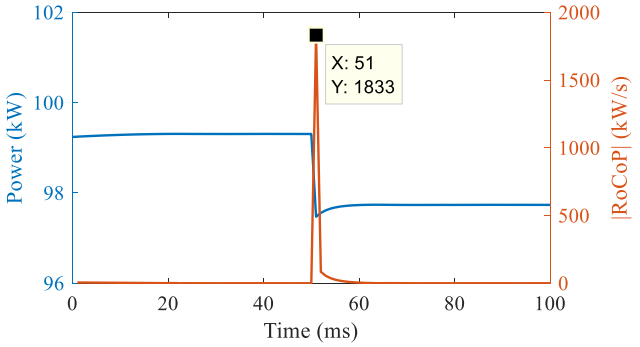

FIGURE 37. Measured array power and calculated RoCoP for an intra-string fault with a resistance of 1 Ω at irradiance level of 300 W/m^2.

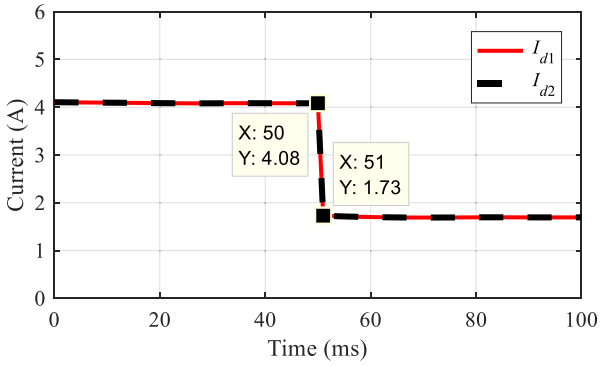

FIGURE 38. Measured differential currents for an intra-string fault with a resistance of 1 Ω at irradiance level of 300 W/m^2.

5) SAMPLING FREQUENCY

A sampling frequency of 1 kHz has been used for data measurements and the method application. This low sampling rate facilitates and reduces the cost of implementing the proposed method. If a higher sampling rate is used for data capturing, the data can then be downsampled digitally to 1 kHz before calculating the RoCoP [28]. However, it is worth testing the method at a sampling rate lower than 1 kHz to account for possible limitations in the measurement capabilities. For this purpose, a sampling frequency of 500 Hz has been used in this section. A shading fault affecting a whole array and intra-string fault cases have been simulated. The RoCoP values for the two cases are shown in Fig. 39 and Fig. 40. As is clear, the RoCoP for the shading fault is less than the RCP_{th}. For the intra-string fault, the RoCoP in Fig. 40 is lower than that in Fig. 15 due to increasing the sampling time. Nevertheless, the RoCoP is much higher than the RCP_{th}. Accordingly, the proposed method successfully works at a lower sampling frequency.

C. EXTENSIVE TESTING

To evaluate the performance of the proposed method, faults of different types have been imposed at various test conditions. The evaluation considered changing the mismatch level where the mismatch level was as low as one module in the fault path. Eight different fault resistance values of 0.001, 1, 3, 5, 10, 20, 30, and 40 Ω have been used. In [19], a fault with a resistance of 30 Ω has been considered as a high impedance

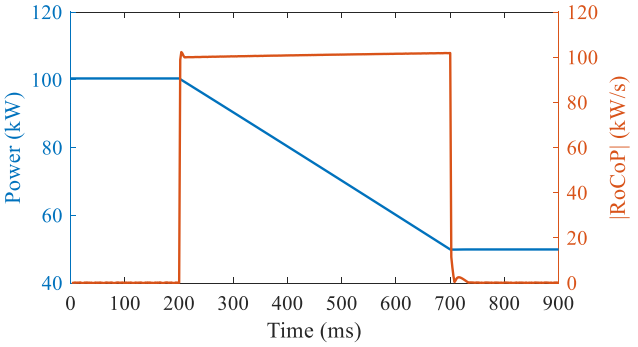

FIGURE 39. Measured array power and calculated RoCoP for shading fault affecting a whole array at a sampling frequency of 500 Hz.

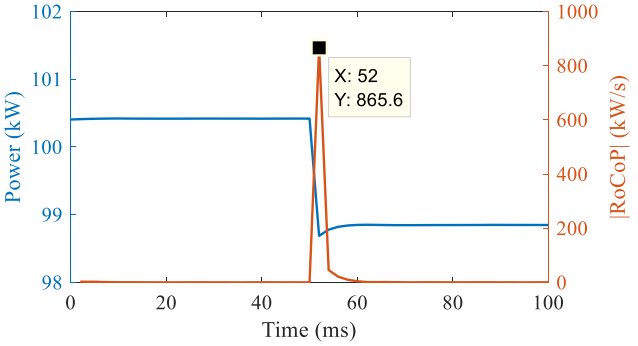

FIGURE 40. Measured array power and calculated RoCoP for an intra-string fault with a resistance of 1 Ω at a sampling frequency of 500 Hz.

fault. Fig. 41 shows the differential currents recorded after the fault inception by 1 ms for 72 fault cases (24 intra-string faults, 32 string-to-negative (STN) faults, and 16 cross-string faults) at different resistance values and mismatch levels.

Regarding the intra-string faults, the two differential currents are equal and close to the current at the MPP (I_m) for 13 fault cases or lower for the remaining 11 fault cases. The former case corresponds to intra-string HIGH faults, while the latter is classified as an intra-string LOW fault. The differential currents are lower than the current at the MPP for faults involving three modules at a resistance of 30 Ω and 40 Ω, faults involving two modules mismatch at a resistance of 20 Ω, 30 Ω, and 40 Ω, and faults with one module mismatch at fault resistance of 3, 5, 10, 20, 30 and 40 Ω. With increasing the fault resistance and decreasing the mismatch level, most of the string current goes to the system (producing useful output power) while a small portion passes through the fault branch. The current at the MPP is used for the threshold level calculation to distinguish between the HIGH and LOW intra-string faults, as previously explained and mentioned in the method's procedure in Fig. 7.

Unlike the intra-string faults, only one of the differential currents (I_{d1} in Fig. 41 for the simulated faults) has high values compared to the other current for string-to-negative terminal faults, coinciding with the explained concept. Therefore, these faults can be distinguished from other fault types based on the differential current's values. Also, these faults can be classified as HIGH or LOW based on the

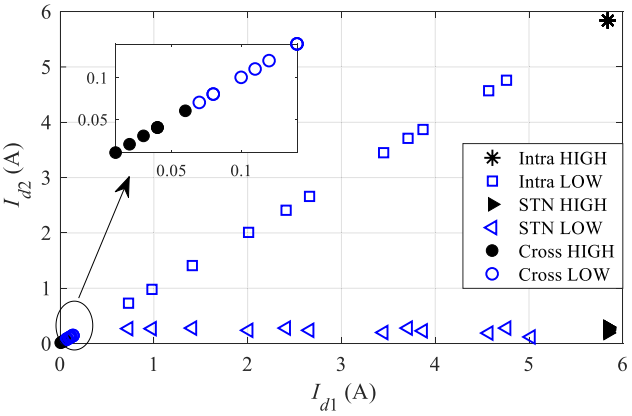

FIGURE 41. Simulation results for different faults (Intra = intra-string, STN = string-to-negative terminal and Cross = cross-string fault).

differential current value compared to the current at the MPP. It is worth noting that values for the two differential currents in Fig. 41 correspond to faults imposed between the string holding currents (I_{11} and I_{12} in Fig. 14) and the negative terminal. In case the fault occurs between the other string that holds currents (I_{21} and I_{22}) and the negative terminal, the values of the differential currents in Fig. 41 will be swapped with each other such that I_{d1} becomes a small value and I_{d2} becomes a high value.

Fig. 41 also shows the results for 16 cross-string faults with mismatch levels of one and two modules (some faults have the same differential currents and appear as a single point in Fig. 41). Unlike the other two fault types, the two differential currents are small, as expected. A threshold value of 0.5 A can distinguish between the cross-string fault and the intra-string fault. With low mismatch and higher fault resistance value, the differential currents increase for cross-string faults, and the fault is classified as a cross-string LOW fault. The threshold level required to differentiate between HIGH and LOW cross-string faults is estimated from testing the system at different conditions. For this case study, a threshold value of 0.07 A is used.

The extensive testing for different fault types shows the uniqueness of the differential currents based on the fault type. The differential currents recorded after the fault inception by 1 ms successfully distinguished between different fault types at different levels of mismatch and different fault resistance values.

Applying the proposed detection and classification scheme requires setting only five parameters as depicted in Fig. 7 (RCP_H, RCP_{th}, I_{th1}, I_{th2}, and I_{th0}). Two of them (RCP_{th} and I_{th0}) are estimated directly from the PV system parameters. Therefore, the proposed method can be generalized for different PV system sizes/ratings without exhausting effort. The following points illustrate how to set different parameters.

- The RCP_{th}, which distinguishes between the shading and short-circuit faults, is calculated assuming a worst-case shading condition results in losing half of the total array power in 0.5 s. Therefore, it is directly calculated from the total array power.

TABLE 2. Comparison with other methods.

	[9]	[12]	[13]	[14]	[15]	[16]	[17]	[18]	[20]	[21]	Proposed
Fault type											
Shading	×	✓	×	✓	✓	✓	✓	✓	✓	✓	✓
Intra-string	✓	✓	✓	✓	✓	✓	✓	✓	✓	✓	✓
STN[a]	✓	✓	✓	✓	×	✓	✓	×	✓	×	✓
Cross-string	✓	×	✓	✓	✓	✓	×	✓	✓	×	✓
Pole-to-pole	×	×	×	×	×	✓	×	×	×	×	✓
Open circuit	×	✓	✓	×	✓	×	×	✓	×	✓	✓
Measurements											
Current sensor	✓	✓	✓	—	✓	✓	✓	—	✓	✓	✓
Voltage sensor	—	✓	✓	✓	—	✓	✓	✓	✓	—	—
Sensors/string	2	1	2	2	1	2	2	2	2	1	1
Operation											
Fs[b] (kHz)	10	*	*	*	1	20	10	1	*	0.01	1
T[c] (ms)	3.9	*	*	*	200	0.4	*	10	*	*	1
Diodes/string	2	×	×	×	1	1	×	—	×	×	1
Irradiance effect	×	×	×	×	×	✓	✓	×	×	×	✓
Training data	✓	✓	✓	✓	—	—	—	—	—	—	—

[a] STN: String-to-negative terminal [b] Fs: Sampling frequency [c] T: Operation time
✓: Considered ×: Not considered —: Not required *: Not specified

- The threshold current (I_{th0}) is calculated by (5), which depends on the rated module current at the maximum power point, and the pre-fault measured differential current. Therefore, it is related to the module rated current and a measured quantity.
- Through modeling the PV system and doing some testing to estimate the maximum possible RoCoP during normal operation due to the implemented MPPT technique, the RCP_H, which distinguishes between normal and fault conditions, can be calculated.
- The threshold current I_{th1} is set based on the maximum possible incremental differential current during cross-string faults. Therefore, it can be defined by simulating cross-string faults at different fault resistance values and mismatch levels. Then, the maximum obtained value for the incremental differential current from this simulation is used to set the current I_{th1}.
- The same simulation cases in the previous point are used to set the threshold current I_{th2}. The simulated cross-string faults are either HIGH or LOW depending on the output current from the faulty string, as discussed in the methodology section. The current I_{th2} is the maximum incremental differential current obtained for the HIGH fault cases.

D. COMPARISON WITH OTHER METHODS

A comparison between the proposed method and some other methods from the literature has been conducted and summarized in Table 2. The comparison considered factors related to the type of faults covered by each method, the type and quantity of sensors required, the sampling frequency for data capturing, the elapsed time before the fault detection and classification, and the number of blocking diodes per string in the PV system construction and noting that the operation time does not include the data processing time.

Compared to the other methods, the proposed method covered more fault types. The proposed method and the methods in [12], [15], [21] used one sensor per string, decreasing the number of sensors by 50% compared to the remaining methods. It is worth noting that increasing the number of measurement transducers increases the implementation cost in two ways. Firstly, the cost of transducers purchases themselves. Secondly, increasing the cost of the data acquisition system due to the need for more input (often analog) channels to read all the measured signals. The proposed method is faster than the other methods other than [16]. However, a high sampling rate of 20 kHz has been used in [16] compared to 1 kHz in the proposed method.

IV. CONCLUSION

A protection scheme to detect and classify fault types in PV systems has been proposed. The proposed scheme employs the array power and cross-strings differential currents to detect and differentiate between various PV system fault types. Two current transducers have been used to measure the differential currents between the two strings for every two strings. The rate of change of the measured array power has been used to differentiate between shading and short-circuit faults. Then, the differential currents were used to classify the fault type in the case of short-circuit faults. The proposed method used the first sample of during fault data. A sampling frequency of 1 kHz has been used for data capturing. Accordingly, the fault has been detected and classified in 1 ms.

The proposed method has been adapted to detect and classify intra-string faults, string-to-negative terminal faults, cross-string faults, and pole-to-pole faults. Furthermore, the fault was then classified as HIGH or LOW, which reflected the fault severity. The method also detected open circuit faults. The method has been evaluated at different

modules mismatch levels and different fault resistance values up to 40 Ω. The evaluation also considered the effect of low irradiance on the performance of the proposed method. The proposed scheme successfully detected and classified all fault cases but failed to classify the cross-string faults to HIGH and LOW only at reduced irradiance levels. However, the cross-string faults were detected and classified as cross-string but without further classification to HIGH or LOW. The low number of measurements per string required (one measurement in our method) and the fast-operating time (1 ms) compared with the methods in the literature encourage the practical implementation of the proposed method.

ACKNOWLEDGMENT

The author would like to acknowledge the financial support received from Taif University Researchers Supporting Project Number (TURSP-2020/61), Taif University, Taif, Saudi Arabia.

REFERENCES

[1] *Climate Change Act 2008 (2050 Target Amendment) (No. SI 2019 No. 1056)*, HM Government, London, U.K., 2019.
[2] United States Environmental Protection Agency. (Jun. 15, 2021). *Inventory of U.S. Greenhouse Gas Emissions and Sinks: 1990-2019*. [Online]. Available: https://www.epa.gov/ghgemissions/inventory-us-greenhouse-gas-emissions-and-sinks
[3] Department for Business, Energy and Industrial Strategy. (Jun. 15, 2021). *Final UK Greenhouse Gas Emissions National Statistics: 1990-2019*. [Online]. Available: https://www.gov.uk/government/statistics/final-uk-greenhouse-gas-emissions-national-statistics-1990-to-2019
[4] R. M. Elavarasan, G. Shafiullah, S. Padmanaban, N. M. Kumar, A. Annam, A. M. Vetrichelvan, L. Mihet-Popa, and J. B. Holm-Nielsen, "A comprehensive review on renewable energy development, challenges, and policies of leading Indian states with an international perspective," *IEEE Access*, vol. 8, pp. 74432–74457, 2020.
[5] A. Qazi, F. Hussain, N. A. Rahim, G. Hardaker, D. Alghazzawi, K. Shaban, and K. Haruna, "Towards sustainable energy: A systematic review of renewable energy sources, technologies, and public opinions," *IEEE Access*, vol. 7, pp. 63837–63851, 2019.
[6] M. Obi and R. Bass, "Trends and challenges of grid-connected photovoltaic systems—A review," *Renew. Sustain. Energy Rev.*, vol. 58, pp. 1082–1094, May 2016.
[7] N. M. Haegel *et al.*, "Terawatt-scale photovoltaics: Trajectories and challenges," *Science*, vol. 356, no. 6334, pp. 141–143, Apr. 2017.
[8] A. Triki-Lahiani, A. B. Abdelghani, and I. Slama-Belkhodja, "Fault detection and monitoring systems for photovoltaic installations: A review," *Renew. Sustain. Energy Rev.*, vol. 82, pp. 2680–2692, Feb. 2018.
[9] I. B. M. Taha, N. I. Elkalashy, M. Alsharef, N. A. Sabiha, M. K. Metwaly, and E. E. Elattar, "Investigation of diode dynamic effect on fault detection of photovoltaic systems," *Sustain. Energy, Grids Netw.*, vol. 23, Sep. 2020, Art. no. 100389.
[10] H. Momeni, N. Sadoogi, M. Farrokhifar, and H. F. Gharibeh, "Fault diagnosis in photovoltaic arrays using GBSSL method and proposing a fault correction system," *IEEE Trans. Ind. Informat.*, vol. 16, no. 8, pp. 5300–5308, Aug. 2020.
[11] M. Dhimish, V. Holmes, B. Mehrdadi, and M. Dales, "Comparing Mamdani Sugeno fuzzy logic and RBF ANN network for PV fault detection," *Renew. Energy*, vol. 117, pp. 257–274, Mar. 2018.
[12] Z. Chen, F. Han, L. Wu, J. Yu, S. Cheng, P. Lin, and H. Chen, "Random forest based intelligent fault diagnosis for PV arrays using array voltage and string currents," *Energy Convers. Manage.*, vol. 178, pp. 250–264, Oct. 2018, doi: 10.1016/j.enconman.2018.10.040.
[13] A. Hazra, S. Das, and M. Basu, "An efficient fault diagnosis method for PV systems following string current," *J. Cleaner Prod.*, vol. 154, pp. 220–232, Jun. 2017.
[14] M. Dhimish, V. Holmes, B. Mehrdadi, M. Dales, and P. Mather, "Photovoltaic fault detection algorithm based on theoretical curves modelling and fuzzy classification system," *Energy*, vol. 140, pp. 276–290, Dec. 2017.
[15] C. Li, Y. Yang, K. Zhang, C. Zhu, and H. Wei, "A fast MPPT-based anomaly detection and accurate fault diagnosis technique for PV arrays," *Energy Convers. Manage.*, vol. 234, Apr. 2021, Art. no. 113950.
[16] H. A. Abd el-Ghany, A. E. ELGebaly, and I. B. M. Taha, "A new monitoring technique for fault detection and classification in PV systems based on rate of change of voltage-current trajectory," *Int. J. Electr. Power Energy Syst.*, vol. 133, Dec. 2021, Art. no. 107248.
[17] D. S. Pillai and N. Rajasekar, "An MPPT-based sensorless line–line and line–ground fault detection technique for PV systems," *IEEE Trans. Power Electron.*, vol. 34, no. 9, pp. 8646–8659, Sep. 2019.
[18] K. A. Saleh, A. Hooshyar, E. F. El-Saadany, and H. H. Zeineldin, "Voltage-based protection scheme for faults within utility-scale photovoltaic arrays," *IEEE Trans. Smart Grid*, vol. 9, no. 5, pp. 4367–4382, Sep. 2018.
[19] A. Khoshnami and I. Sadeghkhani, "Two-stage power–based fault detection scheme for photovoltaic systems," *Sol. Energy*, vol. 176, pp. 10–21, Dec. 2018.
[20] F. Harrou, Y. Sun, B. Taghezouit, A. Saidi, and M.-E. Hamlati, "Reliable fault detection and diagnosis of photovoltaic systems based on statistical monitoring approaches," *Renew. Energy*, vol. 116, pp. 22–37, Feb. 2018.
[21] G. Chen, P. Lin, Y. Lai, Z. Chen, L. Wu, and S. Cheng, "Location for fault string of photovoltaic array based on current time series change detection," *Energy Procedia*, vol. 145, pp. 406–412, Jul. 2018.
[22] S. R. Madeti and S. N. Singh, "Online fault detection and the economic analysis of grid-connected photovoltaic systems," *Energy*, vol. 134, pp. 121–135, Sep. 2017.
[23] S. Silvestre, S. Kichou, A. Chouder, G. Nofuentes, and E. Karatepe, "Analysis of current and voltage indicators in grid connected PV (photovoltaic) systems working in faulty and partial shading conditions," *Energy*, vol. 86, pp. 42–50, Jun. 2015.
[24] S. Silvestre, M. A. da Silva, A. Chouder, D. Guasch, and E. Karatepe, "New procedure for fault detection in grid connected PV systems based on the evaluation of current and voltage indicators," *Energy Convers. Manage.*, vol. 86, no. 10, pp. 241–249, 2014.
[25] S. Silvestre, A. Chouder, and E. Karatepe, "Automatic fault detection in grid connected PV systems," *Sol. Energy*, vol. 94, pp. 119–127, Jun. 2013, doi: 10.1016/j.solener.2013.05.001.
[26] N. Gokmen, E. Karatepe, B. Celik, and S. Silvestre, "Simple diagnostic approach for determining of faulted PV modules in string based PV arrays," *Sol. Energy*, vol. 86, no. 11, pp. 3364–3377, Nov. 2012.
[27] Mathworks. *400-kW Grid-Connected PV Farm*. [Online]. Available: https://uk.mathworks.com/help/physmod/sps/ug/400-kw-grid-connected-pv-farm-average-model.html
[28] A. V. Oppenheim and R. W. Schafer, *Discrete-Time Signal Processing*. Upper Saddle River, NJ, USA: Prentice-Hall, 1999.

F. M. ABOSHADY (Member, IEEE) received the B.Sc. and M.Sc. degrees in electrical engineering from Tanta University, Egypt, in 2010 and 2014, respectively, and the Ph.D. degree in electrical and electronic engineering from the University of Nottingham, U.K., in 2019.

He is currently an Assistant Professor with Tanta University. His research interests include fault location strategies, power system protection, and renewable energy systems.

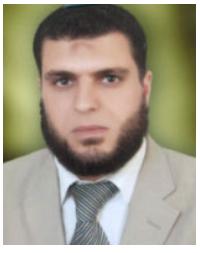

IBRAHIM B. M. TAHA received the B.Sc. degree from the Faculty of Engineering at Tanta, Tanta University, Egypt, in 1995, the M.Sc. degree from the Faculty of Engineering at Mansoura, Mansoura University, Egypt, in 1999, and the Ph.D. degree in electrical power and machines from the Faculty of Engineering, Tanta University, in 2007. Since 1996, he has been a Teaching Staff with the Faculty of Engineering, Tanta University. He is currently an Assistant Professor with the Electrical Engineering Department, Taif University, Saudi Arabia. His research interests include steady state and transient stability of HVDC systems, FACTS, load forecasting, multi-level inverters, dissolved gas analysis, artificial intelligent technique applications, PV system fault detection, and distance adaptive protective relays.